Surface Science 618 (2013) 148–153

Contents lists available at ScienceDirect

Surface Science

journal homepage: www.elsevier.com/locate/susc

Size-dependent quantum diffusion of Gd atoms within Fe nano-corrals

J. Hu [a], R.X. Cao [a], B.F. Miao [a], Z. Liu [a], Z.F. Zhong [a], L. Sun [a], B. You [a], D. Wu [a], W. Zhang [a], An Hu [a], S.D. Bader [b], H.F. Ding [a,*]

[a] National Laboratory of Solid State Microstructures and Department of Physics, Nanjing University, 22 Hankou Road, Nanjing 210093, PR China
[b] Materials Science Division and Center for Nanoscale Materials, Argonne National Laboratory, 9700 S. Cass Avenue, Argonne, IL 60439, USA

ARTICLE INFO

Article history:
Received 16 July 2013
Accepted 29 August 2013
Available online 7 September 2013

Keywords:
Quantum size effect
Nano-corral
Atom diffusion
Scanning tunneling microscopy
Kinetic Monte Carlo simulation

ABSTRACT

We systematically studied the size-dependent quantum diffusion of Gd atoms within Fe circular quantum corrals on Ag(111). By varying the size of the quantum corrals, different types of patterns are observed inside the corrals, including a single dot and circular orbits for the diffusion of Gd adatoms. In addition, the motion of the adatoms also forms circular-like orbits outside the corral. Via quantitative analysis, we confirm that the regions with adatoms' high visiting probability are consistent with the positions of the local electronic density-of-states maxima, both inside and outside the corrals within a <0.2 nm offset. The results agree well with kinetic Monte Carlo simulations that utilize the experimentally determined interaction between Gd and Fe circular corrals. These findings demonstrate that one can engineer adatom motion by controlling the size of the quantum corrals.

1. Introduction

The quantum size effect (QSE) is a fertile topic in low dimensional physics. The QSE can influence various properties, such as growth stability [1–7], optics [8], magnetism [9–11], transport [12], superconductivity [13], surface diffusion [14,15] and molecular transport [16]. These studies mostly focused on quantum confinement in one dimension (1D), more specifically, the vertical direction of films. Additional novel phenomena are expected when electrons are confined in 2D. The QSE is especially pronounced on the close packed (111) surfaces of noble metals, where the electrons can form a 2D free electron gas. Modern experimental techniques, such as scanning tunneling microscope (STM) [17], have been utilized to readily detect such phenomena. These 2D electron gases were reported to mediate long-range adsorbate interactions, which can stabilize atomic superlattices on homogeneous surfaces [18–22]. Quantum confinement of these electrons by static scatterers leads to the formation of patterns in the electronic local density of states (LDOS) [17] and, thus, influences the adsorbate's pinning energy resulting in preferred occupation sites. For instance, 1D confinement of adsorbates is observed within substrate steps [23], strings of atoms [24] and molecular gratings [25]. In 2D cases, studies of CO molecules within self-assembled hexagonal molecular networks [26], and Fe adatoms within self-assembled metal–organic networks [27] demonstrate that the confined LDOS patterns inside cavities play an important role in the preferred occupation sites of adsorbates. In each of these cavities, the CO molecules or the Fe adatoms mainly have one occupation site located at the center. In contrast, inside 30-nm quantum corrals built by STM atomic manipulation, the adatom probability distribution forms several discrete orbits [28,29]. The orbits are closely related to oscillations of the LDOS at the Fermi level (E_F). The studies of 2D systems mentioned above focused on quantum corrals of one fixed size, either a cavity of 4–5 nm [26,27] or a circular corral with the diameter of 30 nm [29]. To better understand the effects and explore potential applications, a systematic size-dependent investigation of confined surface state electronic effects on adatom motion is needed.

In this paper, we systematically studied the size-dependent quantum diffusion of Gd adatoms within Fe nano-corrals on Ag(111). By enlarging the quantum corrals, we obtained single dot, circular orbit, and both patterns for adatoms inside the corrals, in good agreement with the evolution of LDOS near. Moreover, we also observed a circular-like orbit outside the corrals. This further broadens the role of the confinement, in that not only the surface-state electrons confined inside but also those "confined" outside can engineer adatom motion. In addition, to compare with experimental results, the interaction energy between Gd adatoms and the Fe circular corrals is calculated and kinetic Monte Carlo (KMC) simulations are performed. The calculated results are in striking agreement with the experimental findings. Moreover, by taking the real positions of each Fe adatom that forms the corral into consideration, we explain how the deviations of the Fe adatom position in different directions affect the uniformity of the high visiting orbits. Our systematic studies provide strong evidence that one can engineer adatom motion actively by controlling the size of the quantum corrals.

2. Experimental techniques

The experiments were performed in an ultrahigh vacuum chamber (2×10^{-11} mbar) equipped with a low-temperature STM and a sputter

* Corresponding author. Tel.: +86 25 8359 3795; fax: +86 25 8359 5535.
E-mail address: hfding@nju.edu.cn (H.F. Ding).

0039-6028/$ – see front matter © 2013 Elsevier B.V. All rights reserved.
http://dx.doi.org/10.1016/j.susc.2013.08.020

gun. The surface of a high-purity Ag(111) crystal was cleaned by repeated cycles of argon ion sputtering (at 1.5 keV) and annealing (at 870 K). Then the crystal was transferred into the STM stage and cooled to 4.7 K. High-purity Fe and Gd were deposited by means of electron beam evaporation onto the Ag(111) substrate in the STM stage at ≈6 K from thoroughly outgassed rods. The typical rate of deposition was 0.002 monolayer/min. Electrochemically etched tungsten tips were used for the STM measurements. The tips were further cleaned with an electron beam heating device to remove the W-oxide at the tip end [30]. The bias voltage U refers to the sample voltage with respect to the tip. Spectroscopy measurements were performed via the modulation technique utilizing a 10-mV amplitude and 6.09-kHz frequency.

3. Results and discussion

We chose Fe adatoms as the building blocks of the quantum corrals because of the favorable diffusion barrier of ≈43 meV for Fe on Ag(111) [31]. With this magnitude barrier, atomic manipulation can be readily achieved, thus the Fe adatoms can then be immobilized after positioning at 4.7 K. The Ag(111) surface contains a 2D electron gas with a surface-state band that starts at 67 meV below E_F [32]. The scattering of these surface state electrons near point defects and step edges generates standing wave patterns of the electronic density of states [33]. The amplitude of such standing-wave patterns can be greatly enhanced inside the quantum corrals [17]. In our experiments, LDOS patterns due to the quantum interference between electronic waves traveling towards the Fe corral and the backscattered ones were observed. Since the period of oscillation of the LDOS depends only on the Fermi wavelength of the surface, we can tune the LDOS patterns by varying the diameter of the quantum corrals. Fig. 1(a) shows the spatial distribution of the LDOS near E_F within the circular Fe quantum corrals with 6, 10 and 14 nm diameters. The scanning condition for LDOS maps is $U = 20$ mV and $I_t = 1$ nA. Near the Fermi level, the LDOS of Fe atom is considerably lower than that inside the corral. To emphasize the LDOS pattern inside the corral, we adjusted the image contrast and the Fe atoms are therefore almost invisible. To guide the readers, we used the small balls to mark the position of Fe atoms. Inside the quantum corrals, we find an interesting periodic evolution of LDOS as the diameter increases. One spot with high LDOS located at the center of the corral is observed for the 6-nm diameter corral. For the 10-nm diameter corral a circular orbit with high LDOS occurs away from the center while the LDOS at the center is reversed and dips. Further enlarging the corral to 14-nm diameter, we find high LDOS both at the center and away from the center with a circular shape. In addition, we can see separated spots with high LDOS outside the quantum corrals for all three corrals, forming concentric circles, as marked by yellow dash lines. We calculated the LDOS within the three circular corrals by summing up all the standing waves from individual Fe atoms with the formula given in Ref. [33] and find the patterns are similar to the experimental results [Fig. 1(b)]. We note that the slight deviation from the circular symmetry in Fig. 1(a) comes from the imperfect positioning of Fe atoms during the experiments. When we took the real positions in the calculations and the results are in better agreement with the experimental data.

To compare the details, line profiles across the center from the one side to the other of both experiment and calculation are plotted in Fig. 1(c), respectively. The average distance between each corral and the LDOS maximum is given by measuring the diameters of the yellow dashed circles in Fig. 1(a). The experimental first and the nearest orbits with high LDOS are located at a distance $d = 2.6 \pm 0.2$ nm away from the Fe corrals for the three corrals, which is consistent with the calculated values. The distance d, can be estimated via a simple model shown in Fig. 2. When an adatom is acting as a scatterer of surface state electrons, we define the separation between the position of the atom and its first maximum position of the LDOS at E_F as S. Experimentally, S was found to be about 3.2 nm for Ce on Ag(111) [21] and 2.9 nm for Fe on Ag(111) [29]. The difference between them can be attributed to the different scattering phase shift δ_0 caused by different adatoms, which is $\frac{\pi}{2}$ if the adatom is a perfect scatterer for surface electrons. If the corral is formed by dense adatoms like a perfectly continuous circle, as in Ref. [17], $d = S$. In our experiments, we only used a finite number of adatoms to build the quantum corral, thus the situation is slightly different. In order to explain the relation between d and S, a simple model is constructed, as shown in Fig. 2. We used this model to find the superimposed position of the first LDOS maximum between two neighboring Fe adatoms and approximately take this position as the place where the circular orbit is located. The contribution from the other adatoms may lead to variations of the superimposed LDOS intensity at the position. The effect, however, is small when the corral diameter is large because the LDOS decays inversely with the distance from the

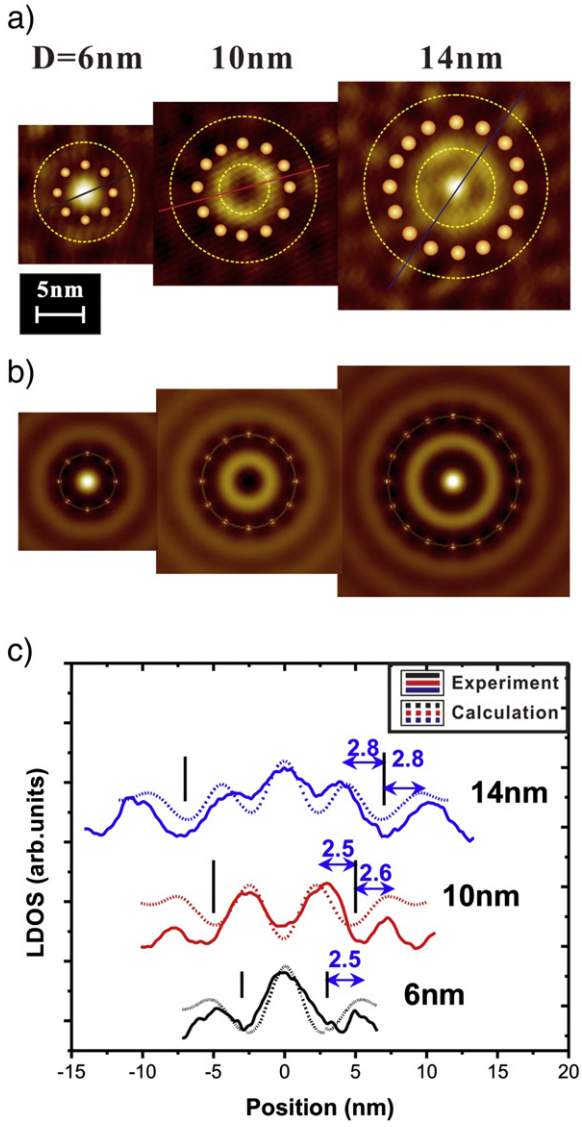

Fig. 1. (a) Experimentally obtained evolution of LDOS near E_F within the corrals. The diameters of Fe corrals (indicated by small balls for clarity) are 6, 10 and 14 nm (from left to right), respectively. Yellow dash lines indicate the position of circular high LDOS inside and outside. (b) Calculated LDOS within the three circular Fe corrals. (c) Experimental and calculated line profiles across corral centers. Fe corral positions are marked as black solid lines, and distances between corral and yellow circles are given.

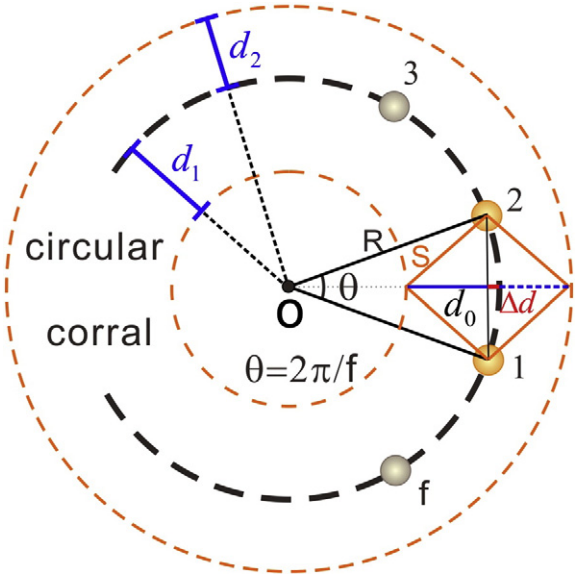

Fig. 2. Schematic model used to estimate the positions of the orbits nearest to the Fe corral for the LDOS and Gd diffusion. Fe atoms with the number of f are indicated by small balls within the black dashed circle. The orange dashed circles refer to the high LDOS or the first minimum position of the LRI inside and outside the corral.

scattering center. For a circular corral of radius R formed by f adatoms with the geometrical relation shown in Fig. 2:

$$d_{1,2} = d_0 \pm \Delta d = \left[S^2 - \left(R \times \mathrm{Sin}\frac{\pi}{f}\right)^2\right]^{1/2} \pm R\left(1 - \mathrm{Cos}\frac{\pi}{f}\right) \quad (1)$$

where d_1 and d_2 represent the distance between the quantum corral and the nearest high LDOS inside and outside, respectively. For a given experimental system, S is fixed. Therefore, d only relates to the radius R and the number of adatoms f. In our experiment, the combinations of R and f are 3 nm with 8 adatoms, 5 nm with 12 adatoms, and 7 nm with 16 adatoms. The distances d calculated from the simple model for corrals of these three corrals are listed in Table 1. To verify this model, we compared each value d with those obtained from the calculated LDOS map [Fig. 1(b)], which takes all adatom contributions into account, and those obtained from our experiment. We find good agreement for d_1 (offset <0.2 nm), and slightly larger deviation for d_2 (offset: 0.3–0.5 nm). The deviations are expected as we only used the overlapping of the standing waves in this simplified model. The real LDOS, however, should be proportional to the square of modulus of the overlapping of wave function. The larger deviation outside the corral can be understood since stronger electronic screening is present due to the geometrical configuration. In addition, we also made the comparison for the circular corral with $R = 15$ nm and $f = 32$ studied in Ref. [29], and the calculated $d_1 = 2.52$ nm with this model agrees with the experimental value of 2.5 nm. Note that this model is also applicable to estimate the first minimum position of the surface-mediated long-range interaction (LRI) of adatoms and the corral (bottom row of Table 1), since it decays as the inverse square of the separation [18].

Table 1
Comparison of values of distance d_1 and d_2 for corrals with different diameters.

Diameter (nm)	6		10		14	
Distance (nm)	d_1	d_2	d_1	d_2	d_1	d_2
LDOS (our model)	2.8	2.4	2.7	2.4	2.8	2.4
LDOS (total adatoms)	–	2.2	2.6	2.2	2.6	2.3
LDOS (experiment)	–	2.5	2.5	2.6	2.8	2.8
Gd diffusion (experiment)	2.7	2.7	2.6	2.7	2.7	2.6

Previous studies showed that quantum confinement of surface state electrons can significantly modify the motion of the adatom [26–29]. Therefore it is expected that different LDOS patterns inside the three quantum corrals will lead to different adatom diffusion behaviors. To identify this, adatom diffusion experiments are carried out in quantum corrals of the sizes discussed above. We chose Gd to study the adatom diffusion within the quantum corrals. Gd adatoms were deposited onto the prepatterned Ag(111) surface as described previously [29]. And we can control the number of the Gd atoms inside the Fe corrals by controlling the Gd dosage and atom manipulation. Gd adatoms have a diffusion barrier of ≈ 7.6 meV and attempt frequency of $\approx 2 \times 10^9$ Hz on Ag(111) [22]. They are mobile and difficult to be observed above 4.7 K. Hence, we cooled the system to <4.4 K for the diffusion studies. Through the measured diffusion barrier and attempt frequency, we can estimate the hopping rates at different temperature by extrapolating the Arrhenius curve. The estimated hopping rate is 14 Hz at 4.7 K and 4 Hz at 4.4 K. To minimize the tip-induced influence, we searched the best tunneling condition by varying the sample bias from −1 to +1 V and the tunneling current from 2 pA to 1 nA. Typically, the tip will push/drag Gd adatoms to the upper half of the corral during scanning if the tip-induced effect is not negligible. In such case, different preferred positions will be found for different scanning directions. We found that there is no apparent tip-induced effect for Gd on Ag(111) when the scanning condition is +0.5 V and 2 pA and the diffusion experiments discussed below were performed under this condition.

We first studied the Gd diffusion within the 6-nm circular Fe quantum corral. To obtain the statistical result, we continued to image the same area of the Fe corral with one Gd adatom inside for several hours. We collected 250 consecutive images and averaged them into a single one. The result is shown in Fig. 3(a). We found that the Gd adatom preferred to stay in the central area inside the corral, similar to the findings in 2D self-assembly network with 4- or 5-nm cavities [26,27]. Apparently, this central area is very close to a region with a high LDOS, as shown in Fig. 1(a). To obtain more quantitative data, we plotted the experimental radial distributions of the visiting probability (red column) in Fig. 4(e). The visiting probability (P) is defined as the normalized frequency that Gd adatoms are observed in one position during its diffusion process. The value of P can be obtained with the formula:

$$P = \frac{n}{N} \times 100\%, \quad (2)$$

in which n refers to the times that Gd adatoms were observed in one position along the radial direction, and N refers to the total times counted inside the corral. For clarity, we also marked the Fe corral position in the figure. Interestingly, we find that the area with high visiting probability for Gd inside actually has a distance about 0.3 nm away from the center. Therefore, the orbit for the Gd adatom at the center is actually a ring with ~0.6-nm diameter even though it is visualized as a single dot in Fig. 3(a). Since it has a broad distribution width of ~1 nm, it could not be resolved in the STM image directly due to the relatively large movement of the Gd adatom (~2 nm) [Inset of Fig. 4(e)].

In order to compare with the experimental results, we performed KMC calculations to simulate the diffusion process of Gd adatoms inside the quantum corral. The method had been used previously for the simulation of Fe superlattice formation on Cu(111) [31]. The KMC parameters, including the LRI between Gd–Gd and Fe–Gd are the same as those in Ref. [29], since our system and experimental conditions are the same except that the corral sizes are different. One Gd adatom was introduced inside the corral with 10^8 hopping events. To make it closer to the experimental conditions, the real experimental position of each Fe adatom is used in the KMC simulation. Both probability distribution [real position: Fig. 3(b); ideal position: inset of Fig. 3(b)] and radial distributed probability [real position: black line in Fig. 4(e); ideal position: blue

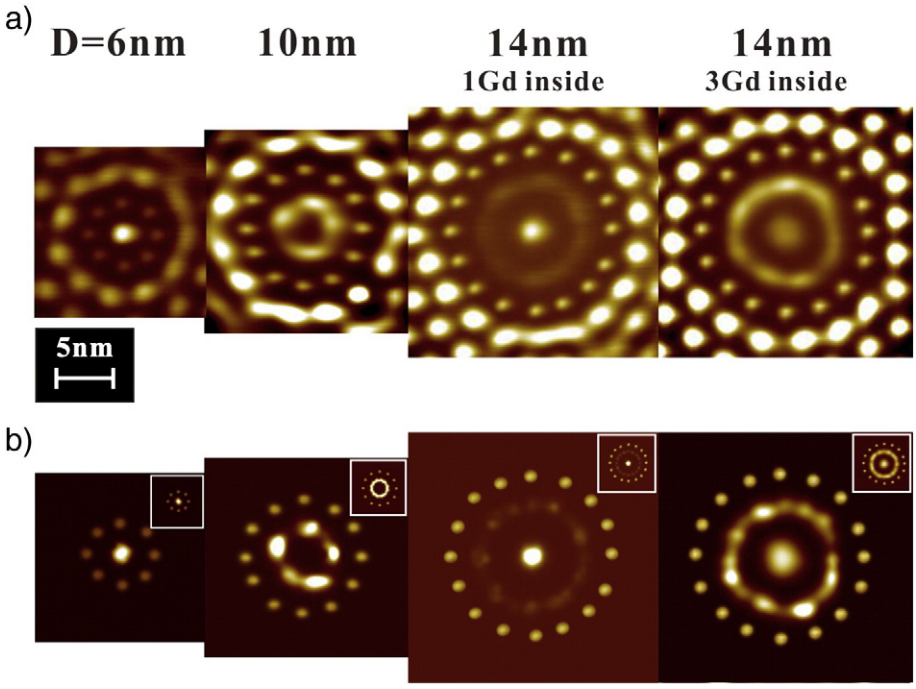

Fig. 3. (a) Experimental probability distribution of Gd adatoms within circular corrals with diameters of 6, 10, 14 nm (1-Gd situation) and 14 nm (3-Gd situation) obtained by averaging 250, 500, 550, 434 consecutive images (from left to right), respectively. (b) Adatom probability distribution of KMC simulations with real positions of corral with 10^8 samplings of corresponding sizes. Inset: KMC simulations for ideal corrals of respective sizes.

line in Fig. 4(e)] show almost identical with experimental data. No obvious difference can be found either in the adatom probability distribution map or the radial distributed probability between KMC simulations with real positions and ideal positions for 6-nm Fe corral.

We found a preferred circular-like distribution (red line) for Gd adatoms that are supposed to walk randomly outside the corral. This can be understood as being due to a concentric circular high LDOS, as shown in Fig. 1(a). Thus, the concept of confinement has a meaning not only for the surface electrons inside the quantum corrals but also for those outside, as long as they are within the influence of the LRI. Even a second circular-like orbit can be observed, though it is much weaker due to the fast decay of the LRI. To understand the underlying mechanism for the Gd distribution outside the corral being separated into several discrete spots, rather than forming a closed and uniform circle, we calculated the distribution map of the interaction energy between the circular corral and a Gd atom by summing up all contributions from the individual Fe atoms constructing the corral [inset of Fig. 4(a)]. In details, we used the experimentally measured distance dependent LRI between a Gd atom and an Fe atom [29]. The sum is calculated according to the individual distance between the position and the Fe atoms constructing the corral. The result presents several separated potential wells outside corresponding to the first minimum in the Gd-corral interaction energy, because of the finite number of Fe atoms used to build the corral. Thus, these separated potential wells act as preferred positions for the Gd adatoms outside. Actually we can see that the regions of the potential wells are close to the separated high LDOS outside the corrals. The line profile along the radial direction, as marked by the red line, is shown in Fig. 4(a). The first and nearest potential minima are ~2.7 nm away from the corral both inside and outside, consistent with those in spatial distributions of high LDOS and high visiting probability of Gd, see also Table 1.

As shown in Fig. 1(a), when a corral is enlarged to 10-nm diameter, a circular high LDOS away from the center occurs. It would be expected that the Gd adatom diffusion inside is different from the situation in a 6-nm corral. Fig. 3(a) also presents the statistical result of ~500 images to show two Gd adatom diffusion inside the 10-nm corral, along with Gd adatoms walking outside. Some positions seem to be more preferable for the Gd adatoms, which is slightly different from the theoretically predicted circular uniform orbit inside [inset of Fig. 3(b)]. This is due to the Fe adatoms in the experiments are not being positioned in a perfect circle, but sometimes have 0.1–0.2 nm deviations in some directions. When we input real positions of each Fe adatom into the KMC without changing other parameters, similar features in the adatom probability distribution are reproduced [Fig. 3(b)].

Similar to what we did in the 6-nm corral situation, we also made a quantitative analysis of the experimental data and the related KMC results [Fig. 4(f)]. The diffusion experiment shows a circular distribution orbit of ~1.5-nm width both inside and outside, with the distance 2.6 ± 0.1 nm away from the corral, corresponding to the two energy minima within the line profile of the calculated interaction potential [Fig. 4(b)]. The radial distributions calculated by KMC in two situations, the ideal circular corral (blue line) and the real one (black line), are also given in the figure. Interestingly, though we found a clear difference in spatial probability distribution inside the circular orbit between the cases for the ideal and imperfect corral, no apparent difference in radial statistics was observed. The position of peak and width of the orbit are almost the same. In detail, the larger deviation of the Fe atoms perpendicular to the radius leads to the greater influence in the uniformity around the circular orbit, while the probability distribution along the radial direction remains almost unchanged.

In the above discussion, we only observed one orbit for Gd adatoms inside both quantum corrals located close to the regions of high LDOS, a dot at the center for 6-nm and a circular orbit away from the center for 10-nm. If there are two regions of high LDOS in, say, a 14-nm corral, how will they influence Gd diffusion? Will two orbits be found? Therefore, we performed similar experiments for a 14-nm corral. We observed that one Gd adatom diffused from the center to a circular-like orbit inside the corral from time to time. After several hours of data collection, the statistical result of 550 images is shown in Fig. 3(a). Besides the dot orbit for Gd adatom at the center, a circular one away from the center was also observed simultaneously. The small deviation in uniformity from that in an ideal circular corral [Inset of Fig. 3(b)] can again be

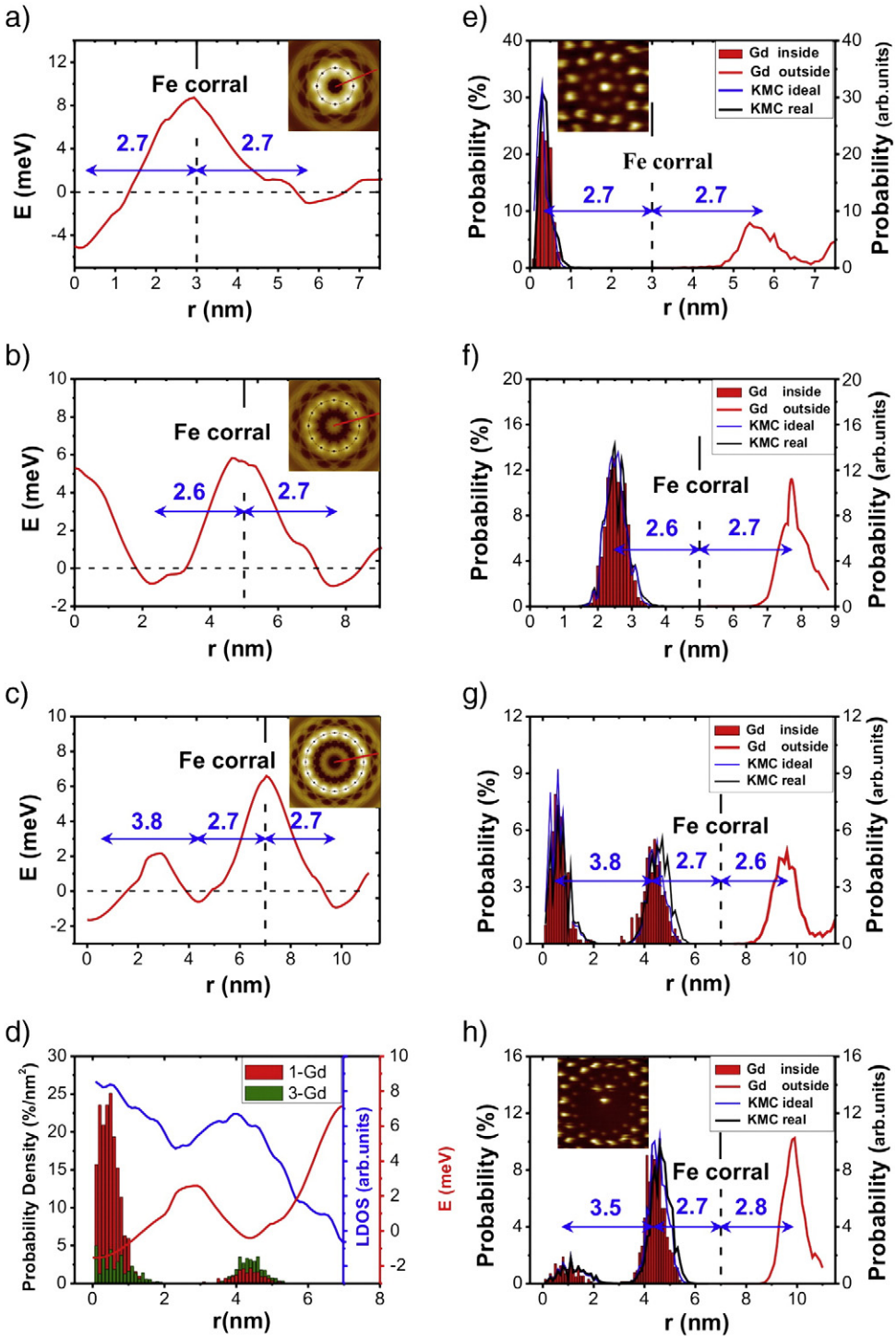

Fig. 4. (a)–(c) Line profiles of the calculated interaction energy map (inset) between a Gd atom and circular corrals. The diameters of the corrals are 6 nm (a); 10 nm (b); 14 nm (c). (d) Probability density inside 14-nm corral with 1-Gd adatom diffusion inside (red column) and 3-Gd adatoms diffusion inside (olive column). The densities are derived from dividing the experimental probabilities in Fig. 4(g) and (h) by area according to Eq. (3). For comparison, a line profile of the LDOS map (blue line) and the Gd-corral interaction energy map (red line) are plotted. (e)–(h) Experimental histograms of the radial distributed probability inside the corral (red column) and for Gd adatoms outside (red line) for corrals with diameters of 6 nm (e); 10 nm (f); 14 nm(1 Gd adatom inside) (g);14 nm (3 Gd adatoms inside) (h). The theoretical radial distribution obtained from KMC simulations, both for ideal corral (blue line) and real corral (black line) are also plotted. Inset of Fig. 4(e) and (h): typical image of 1-Gd adatom diffusion inside 6-nm corral and 3-Gd adatoms inside 14-nm corral.

explained simply by taking real positions of each Fe adatoms in the KMC simulations. Quantitative analysis shows almost perfect matches in both the position of the peak and the intensity between experiment (red columns) and KMC simulations (black line), as presented in Fig. 4(g). Similar to the case for the 6-nm corral, we find that the orbit at the center for Gd adatoms is actually a ring with ~1.0 nm diameter. In order to check the detailed influence caused by the deviations, the statistics of two KMC situations, meaning the ideal corral and real corral, are compared again. This time, however, the circular orbit of the ideal corral obtained from the KMC is ~0.1–0.2 nm thinner than that of the real corral. This is because the deviation in real positions of Fe adatoms along the radial directions is larger than for the case of the 10-nm corral

mentioned above. Therefore, a smaller influence in the uniformity of the circular orbit, but a slightly larger influence in the radial distribution is obtained. In addition, besides the 2.7-nm distance between the first high LDOS and the corral, a 3.8-nm separation between the two neighbor orbits also agrees well with previous studies, which correspond to half of the Fermi wavelength of the Ag (111) surface state [29]. The Gd adatoms outside seem to be trapped there forming an extra Gd circular corral, similar to the novel ring-like structure found inside the corral in our previous study [29]. Moreover, the line profile of the calculated interaction energy map [inset of Fig. 4(c)] shows the corresponding evolution of the energy minimum [Fig. 4(c)]. The regions of three energy minima clearly correspond to the high visiting probability of Gd observed in diffusion experiment and close to the spatial LDOS pattern.

To explore the role of Gd–Gd interaction when more than one orbit exists, we further studied the situation for 3 Gd adatoms diffused inside the 14-nm corral. The statistical result of 434 images is shown in Fig. 3(a) for comparison. We still found 2 distributed orbits of 3 Gd adatoms from both experimental and related KMC simulation results [Fig. 3(b)]. What is different from the 1-Gd situation is that the relative probability of the two orbits has apparently changed and the orbit at the center seems to be larger. From the experimental radial histograms shown in Fig. 4(h), we find that the orbit at the center for Gd adatoms is actually a ring with ~1.6 nm diameter. While the position of the circular orbit stay unchanged relative to the circular corral, thus the separation of the two orbits reduces to 3.5 nm. This distance is smaller than 3.8 nm, which is both theoretically obtained and experimentally observed as a result of Gd-corral interaction only. As shown in inset of Fig. 4(h), during the diffusion process, we often observed that once 1 of 3 Gd occupied the central region the other two preferred to form a triangle shape with it in the circular orbit. This can be attributed to the Gd–Gd interaction which prefers a ~3.0 nm neighboring separation. The competition of the LRI between the central Gd adatom and Fe corral and the Gd–Gd interaction yields a balanced separation of 3.5 nm between the two orbits as also observed in the radial histogram of KMC simulations.

Since two orbits were observed inside the 14-nm corral, it would be interesting to explore and understand their relative occupations for Gd adatoms, especially the experimental results for 1-Gd and 3-Gd are apparently different. To do this, we further calculated the probability density $(\overline{P})$ for either orbit:

$$\overline{P} = \frac{P}{2\pi r \times \Delta r} \tag{3}$$

$\overline{P}$ is the probability we show above and r refers to corresponding radial position. We plotted the probability density along the radial direction ($\Delta r = 0.1$ nm) in Fig. 4(d). We find that actually the dot orbit is much more preferable for Gd than the circular one when just 1 Gd diffuses inside, which is consistent with the fact that the energy minimum is lower and the LDOS is higher at the center. As to the 3-Gd situation, the central dot orbit is only allowed to be occupied by 1 Gd due to the strong repulsion between Gd at shorter distance. Therefore, the other two Gd have to reside in the circular orbit if the central one is taken. In such case, the probably density of the circular orbit is much more enhanced. Interestingly, we find the experimental results can be well reproduced by the KMC simulations when both the Fe–Gd and Gd–Gd interactions are taken into account.

4. Summary

In summary, we performed a systematic study of size-dependent quantum diffusion of Gd atoms within the Fe circular quantum corrals. Inside 6-, 10- and 14-nm quantum corrals, we observed dot, circular, and a combination of both orbits for Gd adatom diffusion, respectively. Via quantitative analysis, we confirmed that the regions of minima in the adatom-corral interaction energy correspond to diffusion orbits for adatoms, and they are closely related to the area with high LDOS within an offset of <0.2 nm. Moreover, we observed that the Gd adatoms walking outside form an extra Gd circular corral under the confinement effect. When the real geometries of the circular corrals are taken into account, KMC simulations can reproduce features that are similar to the experimental result. In detail, we find that the Fe adatom position deviations perpendicular to the radial direction influence the uniformity of the diffusion orbits, while deviations along the radial direction influence their radius. Our study demonstrates that one can engineer adatom motion by tuning the size of quantum corrals.

Acknowledgments

The work at Nanjing is supported by the State Key Program for Basic Research of China (Grant No. 2010CB923401), the NSFC (Grants Nos. 11023002 and 11374145), the Natural Science Foundation of Jiangsu (Grant No. BK2012300), and the PAPD. The work at Argonne is supported by the U.S. Department of Energy, Office of Science, Basic Energy Sciences, under contract No. DE-AC02-06CH11357.

References

[1] B.J. Hinch, C. Koziol, J.P. Toennies, G. Zhang, Europhys. Lett. 10 (1989) 341.
[2] A.R. Smith, K.-J. Chao, Q. Niu, C.-K. Shih, Science 273 (1996) 226.
[3] Z. Zhang, Q. Niu, C.-K. Shih, Phys. Rev. Lett. 80 (1998) 5381.
[4] L. Gavioli, K.R. Kimberlin, M.C. Tringides, J.F. Wendelken, Z. Zhang, Phys. Rev. Lett. 82 (1999) 129.
[5] V. Yeh, L. Berbil-Bautista, C.Z. Wang, K.M. Ho, M.C. Tringides, Phys. Rev. Lett. 85 (2000) 5158.
[6] D.A. Luh, T. Miller, J.J. Paggel, M.Y. Chou, T.C. Chiang, Science 292 (2001) 1131.
[7] M.M. Özer, Y. Jia, B. Wu, Z. Zhang, H.H. Weitering, Phys. Rev. B 72 (2005) 113409.
[8] F. Hache, D. Ricard, C. Flytzanis, J. Opt. Soc. Am. B 3 (1986) 1647.
[9] F. Liu, S.N. Khanna, P. Jena, Phys. Rev. B 42 (1990) 976.
[10] Z.Q. Qiu, J. Pearson, A. Berger, S.D. Bader, Phys. Rev. Lett. 68 (1992) 1398.
[11] J. Li, M. Przybylski, F. Yildiz, X.D. Ma, Y.Z. Wu, Phys. Rev. Lett. 102 (2009) 207206.
[12] N.D. Lang, P. Avouris, Phys. Rev. Lett. 81 (1998) 3515.
[13] Y. Guo, Y.-F. Zhang, X.-Y. Bao, T.-Z. Han, Z. Tang, L.-X. Zhang, W.-G. Zhu, E.G. Wang, Q. Niu, Z.Q. Qiu, J.-F. Jia, Z.-X. Zhao, Q.-K. Xue, Science 306 (2004) 1915.
[14] T.L. Chan, C.Z. Wang, M. Hupalo, M.C. Tringides, K.M. Ho, Phys. Rev. Lett. 96 (2006) 226102.
[15] L.-Y. Ma, L. Tang, Z.-L. Guan, K. He, K. An, X.-C. Ma, J.-F. Jia, Q.-K. Xue, Y. Han, S. Huang, F. Liu, Phys. Rev. Lett. 97 (2006) 266102.
[16] S.-W. Hla, K.-F. Braun, B. Wassermann, K.-H. Rieder, Phys. Rev. Lett. 93 (2004) 208302.
[17] M.F. Crommie, C.P. Lutz, D.M. Eigler, Science 262 (1993) 218.
[18] P. Hyldgaard, M. Persson, J. Phys. Condens. Matter 12 (2000) L13.
[19] J. Repp, F. Moresco, G. Meyer, K.-H. Rieder, P. Hyldgaard, M. Persson, Phys. Rev. Lett. 85 (2000) 2981.
[20] N. Knorr, H. Brune, M. Epple, A. Hirstein, M.A. Schneider, K. Kern, Phys. Rev. B 65 (2002) 115420.
[21] F. Silly, M. Pivetta, M. Ternes, F. Patthey, J.P. Pelz, W.-D. Schneider, Phys. Rev. Lett. 92 (2004) 016101.
[22] R.X. Cao, X.P. Zhang, B.F. Miao, Z.F. Zhong, L. Sun, B. You, A. Hu, H.F. Ding, Surf. Sci. 610 (2013) 65.
[23] H.F. Ding, V.S. Stepanyuk, P.A. Ignatiev, N.N. Negulyaev, L. Niebergall, M. Wasniowska, C.L. Gao, P. Bruno, J. Kirschner, Phys. Rev. B 76 (2007) 033409.
[24] N.N. Negulyaev, V.S. Stepanyuk, L. Niebergall, P. Bruno, W. Hergert, J. Repp, K.-H. Rieder, G. Meyer, Phys. Rev. Lett. 101 (2008) 226601.
[25] Y. Pennec, W. Auwärter, A. Schiffrin, A. Weber-Bargioni, A. Riemann, J.V. Barth, Nat. Nanotech. 2 (2007) 99.
[26] Z. Cheng, J. Wyrick, M. Luo, D. Sun, D. Kim, Y. Zhu, W. Lu, K. Kim, T.L. Einstein, L. Bartels, Phys. Rev. Lett. 105 (2010) 066104.
[27] M. Pivetta, G.E. Pacchioni, U. Schlickum, J.V. Barth, H. Brune, Phys. Rev. Lett. 110 (2013) 086102.
[28] V.S. Stepanyuk, N.N. Negulyaev, L. Niebergall, R.C. Longo, P. Bruno, Phys. Rev. Lett. 97 (2006) 186403.
[29] R.X. Cao, B.F. Miao, Z.F. Zhong, L. Sun, B. You, W. Zhang, D. Wu, A. Hu, S.D. Bader, H.F. Ding, Phys. Rev. B 87 (2013) 085415.
[30] H.F. Ding, J.E. Pearson, D. Li, R. Cheng, F.Y. Fradin, S.D. Bader, Rev. Sci. Instrum. 76 (2005) 123703.
[31] X.P. Zhang, B.F. Miao, L. Sun, C.L. Gao, A. Hu, H.F. Ding, J. Kirschner, Phys. Rev. B 81 (2010) 125438.
[32] J. Li, W.D. Schneider, R. Berndt, Phys. Rev. B 56 (1997) 7656.
[33] M.F. Crommie, C.P. Lutz, D.M. Eigler, Nature 363 (1993) 524.